Overload Capability of the Modular Multilevel Matrix Converter for Feeding High Torque Low Speed Drives

Felix Kammerer, Mario Gommeringer, Johannes Kolb[2], Michael Braun
Karlsruhe Institute of Technology (KIT), Elektrotechnisches Institut (ETI), Germany
felix.kammerer@kit.edu, mario.gommeringer@kit.edu, michael.braun@kit.edu
[2]Schaeffler Technologies GmbH & Co. KG - SHARE at KIT, johannes.kolb@schaeffler.com

Abstract

In drive systems, the semiconductors of conventional converters must be dimensioned for the maximum torque. This results in a converter oversizing even for short time overload requirements near standstill, e.g. for mills in the mining industry. In contrast, the Modular Multilevel Matrix Converter (M3C) is characterized by the ability to share the installed switching power between the input and output side. Hence an overload capability up to 200% of the nominal value can be reached at low speeds without additional efforts. This paper explains how the overload capability is used and analyzes the overload torque limits in the whole speed range.

1. Introduction

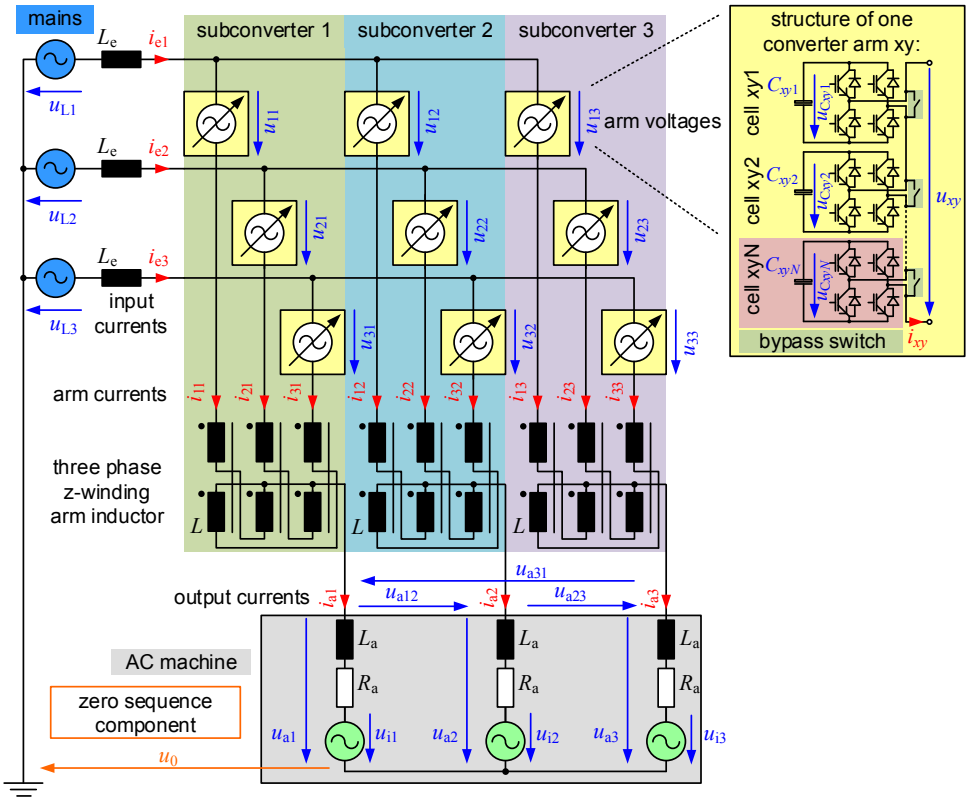

Fig. 1: Modular Multilevel Matrix Converter (M3C) for feeding high torque variable speed drives. The M3C converter arms consist of N series connected H-bridges with a DC-capacitor C_{xyz}.

Fig. 1 shows the Modular Multilevel Matrix Converter (M3C) feeding a high torque variable speed drive. It performs a direct three-phase AC to AC voltage conversion in the medium voltage range and is especially suitable for applications with low nominal machine frequencies [1]. These occur in machines with large diameters and low rotational speeds, for example gear less mills in the mining industry [2]. The M3C can replace thyristor based line commutated cycloconverters used today due to its modular and scalable structure. Classical filter arrangements for the grid connection are dispensable because of the M3C's high voltage quality on the input and output side. This also minimizes additional oscillatory torque caused by harmonics, resulting in less mechanical machine failures [3], lower machine losses and less noise. Therefore maintenance and energy costs can be saved compared to classical drive solutions.

Another important requirement for industry applications is a high availability of the converter to allow continuous production processes. Here the M3C offers the possibility to continue operation after cell failures by short-circuiting faulty cells with a bypass switch (Fig. 1). This reduces the output voltages $u_{\mathrm{a}y}$ (y = output phase number, $y \in \{1, 2, 3\}$) and output power P_{a}. Redundancy cells can be installed to avoid the output voltage reduction depending on the application requirements.

The dimensioning of the semiconductors of line commutated cycloconverters or self commutated three-phase bridges is based on the maximum output currents $i_{\mathrm{a}y}$. The output currents are defined by the maximum torque for a given application. For example, mills in the mining industry require a breakaway torque of at least 120% of the nominal torque [2]. Here the current rating of the converter must be oversized for these short time overloads near standstill. In contrast to this, the M3C can share the installed switching power between the input and output side. At low nominal speeds, the input currents $i_{\mathrm{e}x}$ (x = input phase number, $x \in \{1, 2, 3\}$) are low because of the low active power $P_{\mathrm{e}} = P_{\mathrm{a}}$ transferred to the load. The remaining current capability of the converter arms can be used for higher output currents $i_{\mathrm{a}y}$ to achieve a higher torque without an oversizing of the M3C.

In this paper, the function and the control of the M3C are explained. After that, the overload torque capability of the M3C is analyzed for the whole speed range. The limit of the output currents $i_{\mathrm{a}y}$ for given maximum arm currents $\hat{I}_{xy}$ are calculated and the influences on the cell capacitors C_{xyz} are discussed. Finally, experimental results with a low voltage laboratory prototype with $N = 5$ cells per arm demonstrate the operating performance and the overload capability of the M3C.

2. Structure, fundamentals and control of the M3C

The overall system including the three-phase AC grid, the Modular Multilevel Matrix Converter (M3C) and the three-phase machine is shown in Fig. 1. The M3C consists of three subconverters, with each of them connecting the three input phases via three converter arms and a three phase z-winding arm inductor L to one output phase. As can be seen from Fig. 1, the converter arms are modeled as controllable voltage sources and consist of N series connected cells. They are realized as H-bridges with a capacitor C_{xyz} (z = cell number, $z \in \{\mathbb{N} | 1 \leq z \leq N\}$). By switching the transistors of the cells, each arm is able to generate an adjustable arm voltage u_{xy} with $2N + 1$ voltage steps. The specific voltage range of the arms involving at least one cell with pulse width modulation (PWM) is [4]:

$$-u_{\mathrm{C}xy} = -\sum_{z=1}^{N} u_{\mathrm{C}xyz} \leq u_{xy} \leq \sum_{z=1}^{N} u_{\mathrm{C}xyz} = u_{\mathrm{C}xy} \tag{1}$$

$u_{\mathrm{C}xy}$ is the arm capacitor voltage which is equal to the sum of all cell capacitor voltages $u_{\mathrm{C}xyz}$ in the arm xy. The arm capacitor voltages $u_{\mathrm{C}xy}$ can be split into a constant average value $\overline{u}_{\mathrm{C}xy}$ corresponding to the mean capacitor energy $\overline{w}_{\mathrm{C}xy}$ stored in the converter arms and a time-variant part $\tilde{u}_{\mathrm{C}xy}$ which depends on the energy pulsation $\tilde{w}_{\mathrm{C}xy}$ caused by the actual arm power $p_{xy} = u_{xy} \cdot i_{xy}$:

$$u_{\mathrm{C}xy} = \tilde{u}_{\mathrm{C}xy} + \overline{u}_{\mathrm{C}xy} \approx \frac{N}{C_{xyz} \cdot \overline{u}_{\mathrm{C}xy}} \int p_{xy} \mathrm{d}t + \overline{u}_{\mathrm{C}xy} = \frac{N}{C_{xyz} \cdot \overline{u}_{\mathrm{C}xy}} \int u_{xy} i_{xy} \mathrm{d}t + \overline{u}_{\mathrm{C}xy} \tag{2}$$

To maintain a constant average arm capacitor voltage $\overline{u}_{\mathrm{C}xy}$, the control system has to ensure that the average arm power $\overline{p}_{xy}$ is zero for all nine converter arms. The cell capacitors C_{xyz} are dimensioned to buffer the maximum energy pulsation Δw without exceeding a maximum allowable arm capacitor voltage pulsation Δu_{C}. A detailed analysis of the arm power p_{xy} with the corresponding arm voltage u_{xy} and current i_{xy} can be found in [5]. Neglecting the voltages across the inductors, the arm voltages u_{xy} can be approximated to:

$$u_{xy} \approx u_{\mathrm{L}x} - u_{\mathrm{a}y} - u_0 \tag{3}$$

According to (3) the arm voltages u_{xy} are composed by the input voltages $u_{\mathrm{L}x}$, the output voltages $u_{\mathrm{a}y}$ and the zero sequence voltage u_0. With (1) and assuming sinusoidal voltages, the minimum arm capacitor voltage $u_{\mathrm{C}xy,\mathrm{min}}$ can be calculated depending on the arm voltage amplitude $\hat{U}_{xy}$:

$$u_{\mathrm{C}xy,\mathrm{min}} \geq \hat{U}_{xy} \approx \hat{U}_{\mathrm{L}} + \hat{U}_{\mathrm{a}} + \hat{U}_0 \tag{4}$$

The arm currents i_{xy} are composed of one third of the phase input currents $i_{\mathrm{e}x}$, one third of the phase output currents $i_{\mathrm{a}y}$ and two internal diagonal currents $i_{\mathrm{d}1xy}$ and $i_{\mathrm{d}2xy}$:

$$i_{xy} = \frac{i_{\mathrm{e}x}}{3} + \frac{i_{\mathrm{a}y}}{3} + i_{\mathrm{d}1xy} + i_{\mathrm{d}2xy} \tag{5}$$

The two internal diagonal currents $i_{\mathrm{d}1xy}$ and $i_{\mathrm{d}2xy}$ are used for the internal power distribution [5]. They do not occur neither on the input nor the output side of the M3C. With (5) and assuming sinusoidal currents, the arm current amplitude $\hat{I}_{xy}$ which defines the current capability of the semiconductors can be calculated to:

$$\hat{I}_{xy} = \frac{\hat{I}_{\mathrm{e}}}{3} + \frac{\hat{I}_{\mathrm{a}}}{3} + \hat{I}_{\mathrm{d}1} + \hat{I}_{\mathrm{d}2} \tag{6}$$

The four current components can be calculated from the measured arm currents using the $\alpha\beta0$-transformations from [5] and can be independently controlled with the control scheme presented in [4, 6]. A superposed energy control maintains the average value of the nine arm capacitor voltages $u_{\mathrm{C}00}$ at a constant level. This is realized by adjusting the input current amplitude $\hat{I}_{\mathrm{e}}$ in order to achieve an equal active input and output power $P_{\mathrm{e}} = P_{\mathrm{a}}$:

$$\hat{I}_{\mathrm{e}} = \frac{\hat{U}_{\mathrm{a}} \cdot \cos(\varphi_{\mathrm{a}})}{\hat{U}_{\mathrm{e}} \cdot \cos(\varphi_{\mathrm{e}})} \cdot \hat{I}_{\mathrm{a}} \tag{7}$$

φ_{a} is the phase angle between the output voltage $\hat{U}_{\mathrm{a}}$ and current $\hat{I}_{\mathrm{a}}$ and φ_{e} is the phase angle between the input voltage $\hat{U}_{\mathrm{e}}$ and current $\hat{I}_{\mathrm{e}}$. The differences between the average values of the nine arm capacitor voltages $\overline{u}_{\mathrm{C}xy}$ are controlled by the balancing control using four balancing directions obtained from the measured arm capacitor voltages $u_{\mathrm{C}xy}$ by $\alpha\beta0$-transformations [4, 5, 6]. Here, the internal diagonal currents $i_{\mathrm{d}1xy}$ and $i_{\mathrm{d}2xy}$ are used to generate active power components in each of the four directions allowing an energy exchange between all nine converter arms for the balancing task. At critical operating points, the zero sequence voltage u_0

is used. This allows an operation even if the absolute input and output angular frequencies are equal, $|\omega_\mathrm{a}| = \omega_\mathrm{e}$ [5]. In this paper, the internal currents and the zero sequence voltage are neglected in the following calculations due to their low values at normal operation.

Further details about the M3C can be found in the literature. [1] calculates the installed switching power of the M3C. [7] explains the advantages and material savings of the three phase z-winding arm inductors L compared to nine individual arm inductors. An alternative control scheme which includes methods to reduce the energy pulsation is presented in [8] with the corresponding experimental results [9]. The benefits of feeding the rotor circuit of a Doubly Fed Induction Generator (DFIG) by the M3C are explained in [10]. This variable speed generator system increases the part load efficiency and dynamics compared to grid connected synchronous generators and can be used in variable speed pump storage power plants and wind turbines.

3. Calculation of the Overload Output Current Capability

In this Section, the output current capability of the M3C is analyzed in the whole speed range to explain the overload capability. The calculations are exemplary done in a normalized manner for a synchronous machine excited by a DC field current operating with $\cos(\varphi_\mathrm{a}) = 1$. This machine type is widely used for applications with large diameters and low rotational speeds [2, 3]. The nominal output angular frequency $\omega_\mathrm{a,n}$ is selected to 40% of the input angular frequency ω_e, at this point the output voltage amplitude $\hat{U}_\mathrm{a}$ is equal to the input voltage amplitude $\hat{U}_\mathrm{e}$.

Fig. 2 shows the operation with constant torque up to the nominal point $|\nu| = 0.4$ and constant power in the field weakening area. ν is the frequency ratio between the input and output angular frequency $\nu = \frac{\omega_\mathrm{a}}{\omega_\mathrm{e}}$. The maximum arm current amplitude $\hat{I}_{xy,\mathrm{n}}$ is reached at the nominal point $|\nu| = 0.4$ and defines the arm current rating of the M3C (Fig. 2a). The maximum arm current amplitude $\hat{I}_{xy,\mathrm{n}}$ is not fully used at low output frequencies $|\nu| < 0.4$ due to the lower active power $P_\mathrm{a} = P_\mathrm{e}$ and therefore lower input current amplitude $\hat{I}_\mathrm{e}$.

The output current amplitude $\hat{I}_\mathrm{a}$ can be further increased at low nominal output frequencies (Fig. 3a) to completely use the maximum arm current amplitude $\hat{I}_{xy,\mathrm{n}}$ in the whole operation range. In this case, the maximum allowable output current amplitude $\hat{I}_{\mathrm{a,max}}$ is calculated by inserting (7) into (6) and neglecting $\hat{I}_{\mathrm{d1}}$ and $\hat{I}_{\mathrm{d2}}$ due to their low values at normal operation:

$$\hat{I}_{\mathrm{a,max}} = \frac{3 \cdot \hat{I}_{xy,\mathrm{n}}}{1 + \frac{\hat{U}_\mathrm{a} \cdot \cos(\varphi_\mathrm{a})}{\hat{U}_\mathrm{e} \cdot \cos(\varphi_\mathrm{e})}} \tag{8}$$

Fig. 3a shows the composition of the arm current amplitude $\hat{I}_{xy} = \hat{I}_{xy,\mathrm{n}}$. At low output frequencies, the output power P_a is low which results in a lower input current amplitude $\hat{I}_\mathrm{e}$. The remaining arm current capability can be used for the output current amplitude $\hat{I}_\mathrm{a} = \hat{I}_{\mathrm{a,max}}$. This results in an increased starting torque capability $T \sim \hat{I}_\mathrm{a}$ of 200% at standstill compared to the nominal operation point which decreases to 133% at half nominal speed ($|\nu| = 0.2$). This behavior is very advantageous in applications which require high breakaway torques in the range from $120 - 150\%$ like mills in the mining industry [2]. A converter oversizing for the starting torque is not necessary by using the M3C.

For operation with constant torque, the arm current rms-values $I_{xy,\mathrm{rms}}$ (Fig. 2b) are always below or equal to the rms-value at the nominal operation point, even for zero output frequency $f_\mathrm{a} = 0$. By increasing the output current amplitude $\hat{I}_\mathrm{a}$ at low frequencies, the arm current

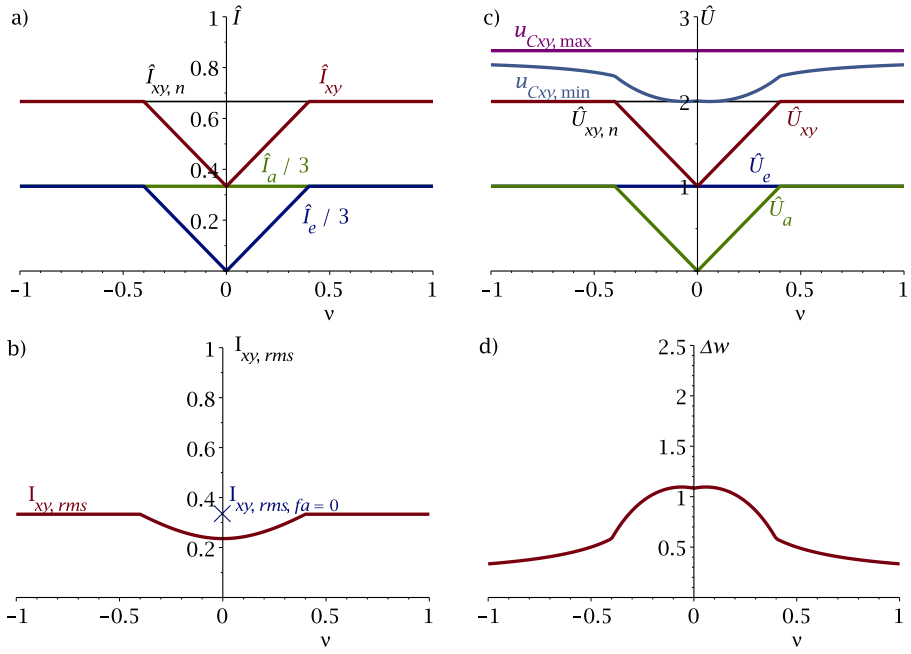

Fig. 2: Operation of a synchronous machine at constant torque below $|\nu| = 0.4$ and constant power above $|\nu| = 0.4$: a) arm current amplitude components $\hat{I}_{xy}$, $\frac{\hat{I}_\mathrm{e}}{3}$, $\frac{\hat{I}_\mathrm{a}}{3}$; b) arm current rms-value $I_{xy,\mathrm{rms}}$; c) arm voltage amplitude components $\hat{U}_{xy}$, $\hat{U}_\mathrm{e}$, $\hat{U}_\mathrm{a}$; d) maximum energy pulsation Δw (all pu values)

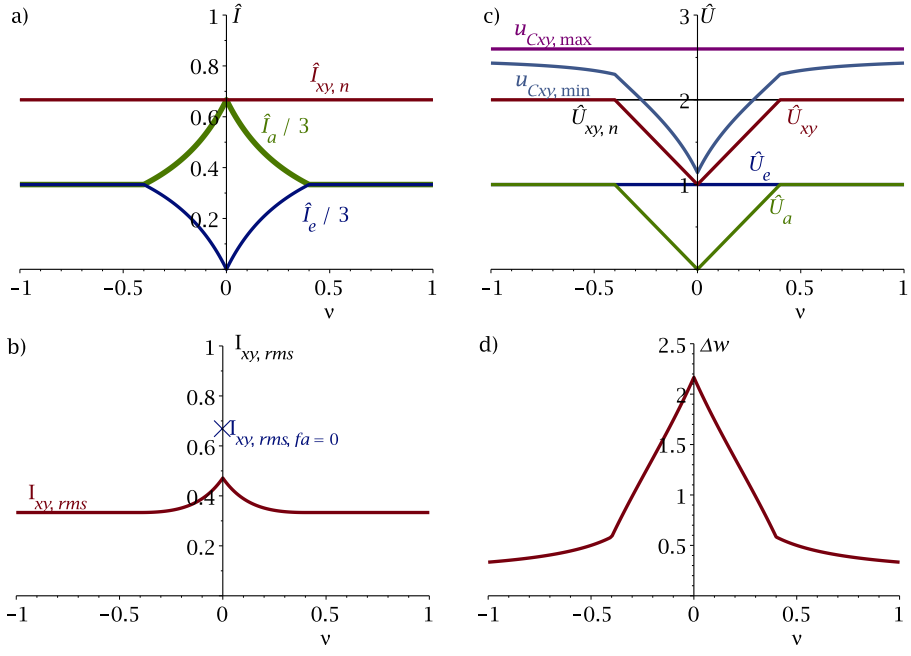

Fig. 3: Operation of a synchronous machine at a constant rated arm current amplitude $\hat{I}_{xy,\mathrm{n}}$: a) arm current amplitude components $\hat{I}_{xy}$, $\frac{\hat{I}_\mathrm{e}}{3}$, $\frac{\hat{I}_\mathrm{a}}{3}$; b) arm current rms-value $I_{xy,\mathrm{rms}}$; c) arm voltage amplitude components $\hat{U}_{xy}$, $\hat{U}_\mathrm{e}$, $\hat{U}_\mathrm{a}$; d) maximum energy pulsation Δw (all pu values)

rms-value $I_{xy,\mathrm{rms}}$ (Fig. 3b) increases up to 200% at standstill compared to the constant torque operation (Fig. 2b). This must be considered in the design of the cooling depending on the duration of the overload.

The maximum energy pulsation Δw for operation with a constant output current amplitude $\hat{I}_{\mathrm{a}}$ is shown in Fig. 2d. This pulsation must be buffered in the cell capacitors C_{xyz}. By selecting a maximum arm capacitor voltage $u_{\mathrm{C}xy,\mathrm{max}} = \Delta u_{\mathrm{C}} + u_{\mathrm{C}xy,\mathrm{min,n}}$ ($u_{\mathrm{C}xy,\mathrm{min,n}}$= nominal minimum arm capacitor voltage), the required cell capacitance can be calculated for the worst case of Δw:

$$C_{xyz} = N \cdot \frac{2\Delta w}{u^2_{\mathrm{C}xy,\mathrm{max}} - u^2_{\mathrm{C}xy,\mathrm{min,n}}} \tag{9}$$

Fig. 2c shows the calculation for $\Delta u_{\mathrm{C}} = 0.3 \cdot u_{\mathrm{C}xy,\mathrm{min,n}} = \hat{U}_{xy,\mathrm{n}}$. Here the nominal minimum arm capacitor voltage $u_{\mathrm{C}xy,\mathrm{min,n}}$ is selected in a way that the nominal output voltage can be reached in the whole operation range. Hence the resulting minimum arm capacitor voltage $u_{\mathrm{C}xy,\mathrm{min}}$ is still higher than the required arm voltage $\hat{U}_{xy}$ in all operation points. This allows a high dynamic voltage reserve, a further reduction of the cell capacitors C_{xyz} or a operation with a reduced average arm capacitor voltage $\overline{u}_{\mathrm{C}xy}$ at low output voltages. This can improve the output voltage quality and reduces switching losses by using smaller cell capacitor voltages $u_{\mathrm{C}xyz}$.

Otherwise it can be used to buffer the higher maximum energy pulsation Δw (Fig. 3d) which occurs for higher output currents at low frequencies. Here a lower minimum arm capacitor voltage $u_{\mathrm{C}xy,\mathrm{min}} \geq \hat{U}_{xy} = \hat{U}_{\mathrm{e}} + \hat{U}_{\mathrm{a}}$ (Fig. 3c) avoids oversizing of the cell capacitors in most cases. The reduced dynamic voltage reserve must be accepted in this case or a higher cell capacitance must be installed. This must be checked for each dimensioning depending on the application requirements. Another possibility is the use of internal diagonal currents, here the energy pulsation is reduced in the overload case, but the output currents limits from Fig. 3a cannot be fully reached.

As result it can be seen that the M3C output current capability can fulfill the overload requirements at low speeds without oversizing of the cell semiconductors. The dimensioning of the cell capacitors can be varied depending on the dynamic requirements.

4. Experimental Results with the Low Voltage Laboratory Prototype

To demonstrate the performance of the M3C, a low voltage laboratory prototype was built up with $N = 5$ cells per arm. The composition of the arm currents at different output frequencies is exemplary shown using an induction machine due to available laboratory equipment. The control method from [6] is used for the independent subordinate current control and the superposed energy and balancing control. The control of the induction machine consists of a superposed speed controller and subordinate current controllers for the field generating current $i_{\mathrm{ad}} = 13\,\mathrm{A}$ and the torque generating current i_{aq}. The induction machine is mechanically coupled to a torque controlled DC-machine working as adjustable load. Fig. 4 shows a measurement result at a speed of $n = 100\,\mathrm{min}^{-1}$. The arm current amplitude $\hat{I}_{xy} \approx 14\,\mathrm{A}$ allows a torque generating current of $i_{\mathrm{aq}} \approx 29\,\mathrm{A}$ due to the low active input current of $i_{\mathrm{ed}} \approx 6\,\mathrm{A}$. At a speed of $n = 1000\,\mathrm{min}^{-1}$ (Fig. 5), the torque generating current is reduced to $i_{\mathrm{aq}} \approx 18\,\mathrm{A}$ to keep the arm current amplitude $\hat{I}_{xy} \approx 14\,\mathrm{A}$ constant due to a higher active input current $i_{\mathrm{ed}} \approx 14\,\mathrm{A}$. Comparing both cases, it can be seen that the torque generating current i_{aq} at $n = 100\,\mathrm{min}^{-1}$ is about $60\,\%$ higher than i_{aq} at $n = 1000\,\mathrm{min}^{-1}$ with the same maximum arm current amplitude $\hat{I}_{xy} \approx 14\,\mathrm{A}$. The values of internal diagonal 1 and 2 currents $i_{\mathrm{d1},\alpha/\beta}$, $i_{\mathrm{d2},\alpha/\beta}$ are very low, because they are only used for balancing the arm capacitor voltages $u_{\mathrm{C}xy}$. The average value $u_{\mathrm{C00}} = 650\,\mathrm{V}$ is kept constant at all speeds. Hence the performance of the M3C for feeding AC machines at a constant maximum arm current amplitude is successfully shown.

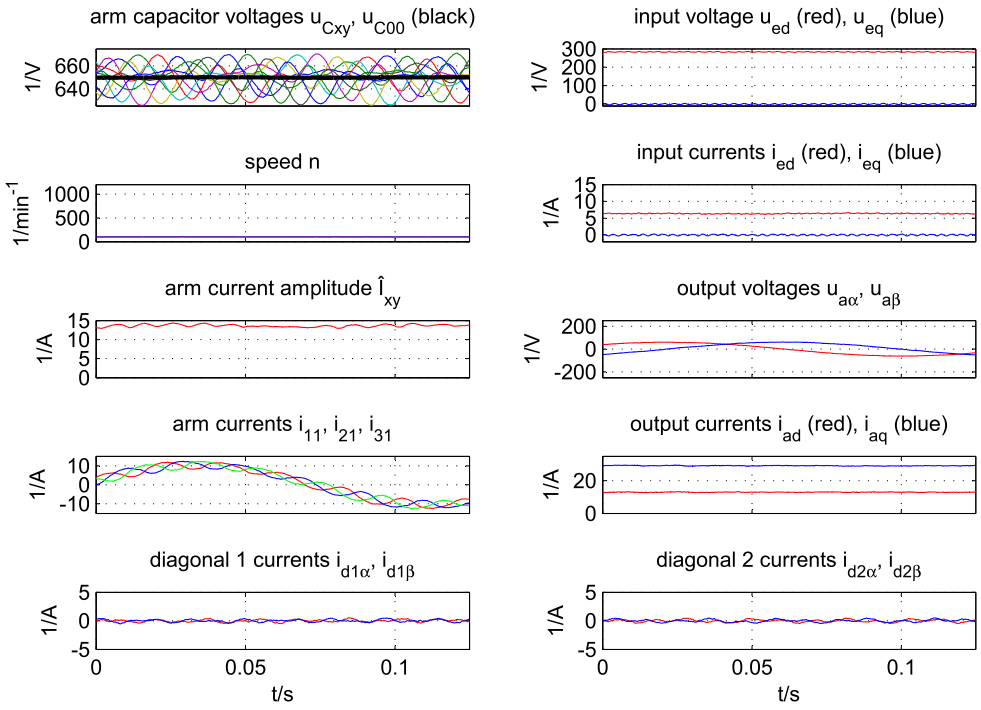

Fig. 4: Measurement of the M3C control variables at a machine speed of $100\,\mathrm{min}^{-1}$, short time averaged values at $t_\mathrm{A} = \frac{1}{f_\mathrm{PWM}} = \frac{1}{8\,\mathrm{kHz}}$.

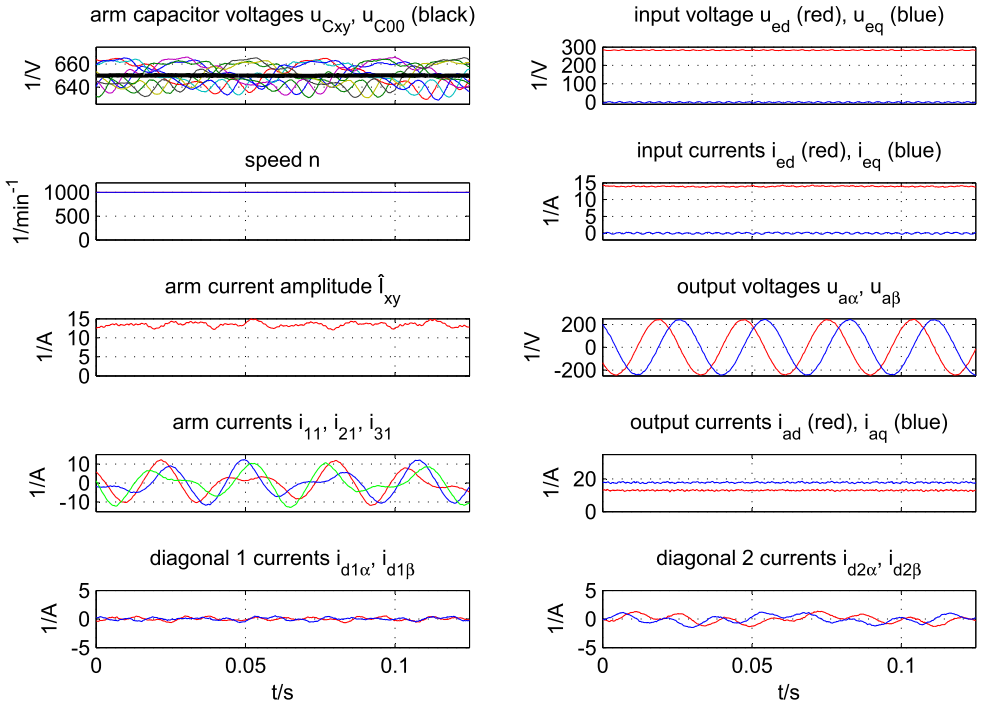

Fig. 5: Measurement of the M3C control variables at a machine speed of $1000\,\mathrm{min}^{-1}$, short time averaged values at $t_\mathrm{A} = \frac{1}{f_\mathrm{PWM}} = \frac{1}{8\,\mathrm{kHz}}$.

5. Conclusion

The intrinsic current overload capability of the Modular Multilevel Matrix Converter (M3C) in the low speed range is explained in detail. The M3C offers a starting torque capability up to 200%

of the nominal value without any electrical oversizing. This is possible due to the fact that the M3C is the unique converter that can use the complete installed switching power either on the input or the output side. Therefore it is especially suitable to replace cycloconverters which are used today in high power medium voltage drive applications like mills which require a high breakaway torque.

6. Acknowledgment

The authors would like to thank the DFG (German Research Foundation) which supports this research project.

7. References

[1] A.J. Korn, M. Winkelnkemper, P. Steimer, and J.W. Kolar. Direct modular multi-level converter for gearless low-speed drives. In *Power Electronics and Applications (EPE 2011), Proceedings of the 2011-14th European Conference on*, pages 1–7, 2011.

[2] J.R. Rodriguez, J. Pontt, P. Newman, R. Musalem, H. Miranda, L. Moran, and G. Alzamora. Technical evaluation and practical experience of high-power grinding mill drives in mining applications. *Industry Applications, IEEE Transactions on*, 41(3):866–874, May 2005.

[3] V. Guerrero and J. Pontt. Oscillatory torque caused by dead time in the current control of high power gearless mills. In *IECON 2011 - 37th Annual Conference on IEEE Industrial Electronics Society*, pages 1966–1970, Nov 2011.

[4] F. Kammerer, J. Kolb, and M Braun. A novel cascaded vector control scheme for the Modular Multilevel Matrix Converter. *IECON 2011 Melbourne*, Nov. 2011.

[5] F. Kammerer, M. Gommeringer, J. Kolb, and M. Braun. Energy balancing of the modular multilevel matrix converter based on a new transformed arm power analysis. In *16th Conference on Power Electronics and Applications, EPE14-ECCE Europe*, Aug 2014.

[6] F. Kammerer, J. Kolb, and M. Braun. Fully decoupled current control and energy balancing of the Modular Multilevel Matrix Converter. *EPE-PEMC 2012 ECCE Europe, Novi Sad, Serbia*, 2012.

[7] F. Kammerer, J. Kolb, and M. Braun. Optimization of the passive components of the Modular Multilevel Matrix Converter for Drive Applications. *PCIM Europe, Nuremberg, Germany*, 2012.

[8] W. Kawamura, M. Hagiwara, and H. Akagi. Control and experiment of a modular multilevel cascade converter based on triple-star bridge cells (mmcc-tsbc). *Industry Applications, IEEE Transactions on*, PP(99):1–1, 2014.

[9] W. Kawamura, M. Hagiwara, and H. Akagi. Experimental verification of a modular multilevel cascade converter based on triple-star bridge-cells (mmcc-tsbc) for motor drives. In *Future Energy Electronics Conference (IFEEC), 2013 1st International*, pages 454–459, Nov 2013.

[10] F. Kammerer, M. Gommeringer, J. Kolb, and M. Braun. Benefits of operating doubly fed induction generators by modular multilevel matrix converters. *PCIM Europe, Nuremberg, Germany*, 2013.